The Astrophysical Journal Letters, 928:L9 (6pp), 2022 March 20 https://doi.org/10.3847/2041-8213/ac5b70

The Composition and Power of the Jet of the Broad-line Radio Galaxy 3C 120

Andrzej A. Zdziarski[1], Dakalo G. Phuravhathu[2], Marek Sikora[1], Markus Böttcher[2], and James O. Chibueze[2,3]
[1] Nicolaus Copernicus Astronomical Center, Polish Academy of Sciences, Bartycka 18, PL-00-716 Warszawa, Poland; aaz@camk.edu.pl
[2] Centre for Space Research, North-West University, Potchefstroom 2520, South Africa
[3] Department of Physics and Astronomy, Faculty of Physical Sciences, University of Nigeria, Carver Building, 1 University Road, Nsukka 410001, Nigeria
Received 2022 February 22; revised 2022 March 7; accepted 2022 March 7; published 2022 March 25

Abstract

We calculated the electron–positron pair-production rate at the base of the jet of 3C 120 due to collisions of photons from the hot accretion flow using the measurement of its average soft gamma-ray spectrum by the Compton Gamma Ray Observatory. We found that this rate approximately equals the flow rate of leptons emitting the observed synchrotron radio-to-IR spectrum of the jet core, calculated using the extended jet model following Blandford & Königl. This coincidence shows the jet composition is likely to be pair dominated. We then calculated the jet power in the bulk motion of ions and found it greatly exceeds that achievable by the magnetically arrested disk scenario for the maximum black hole spin unless the jet contains mostly pairs. Next, we found that the magnetic flux through the synchrotron-emitting jet equals the maximum poloidal flux that can thread the black hole. Finally, we compared two estimates of the magnetization parameter at the onset of the synchrotron emission and found they are in agreement only if pairs dominate the jet content.

Unified Astronomy Thesaurus concepts: Relativistic jets (1390); Non-thermal radiation sources (1119); Accretion (14); Active galaxies (17); Radio galaxies (1343)

1. Introduction

We consider possible mechanisms to produce electron–positron ($e^{\pm}$) pairs at the base of relativistic jets. There are a lot of indications that extragalactic jets contain $e^{\pm}$ pairs dominating their content by number (e.g., Ghisellini 2012; Pjanka et al. 2017; Snios et al. 2018; Sikora et al. 2020; Liodakis et al. 2022). However, it is not clear what the mechanism producing those pairs is.

One possibility is pair production in the ergosphere of a rotating black hole (BH; Blandford & Znajek 1977). If the charge density there is low enough, a strong electric field forms a "spark gap," where electrons are accelerated to relativistic energies. These emit energetic γ-rays by Compton-scattering ambient soft photons. The γ-rays in turn produce $e^{\pm}$ pairs in collisions with ambient photons. However, the electric field will be screened when the charge density in the ergosphere becomes higher than the Goldreich–Julian (Goldreich & Julian 1969) density, $n_{\rm GJ}=\Omega B/2\pi ec$, where Ω is the BH angular velocity, B is the strength of the magnetic field of the magnetosphere, and e is the electron charge. The pairs are produced above the gap (see Figure 1 in Levinson & Rieger 2011) and thus the density there can exceed $n_{\rm GJ}$ by some factor, which Levinson & Rieger (2011) estimate to be $\lesssim 10^3$. As found to follow from that estimate, this mechanism can be efficient in low-luminosity sources (Levinson & Rieger 2011; Mościbrodzka et al. 2011). On the other hand, the electron density close to the BH in blazars has been estimated to be much larger, $\sim(10^{10}$–$10^{13})n_{\rm GJ}$ (Nokhrina et al. 2015). Here we accounted for the synchrotron-emitting electrons only, without counting any background electrons, which Nokhrina et al. (2015) also included. Even without those electrons, it appears unlikely that such high electron densities can be obtained by this process.

An alternative is pair production within the jet base via collisions of energetic photons originating in the accretion flow (Henri & Pelletier 1991; Beloborodov 1999; Levinson & Rieger 2011; Aharonian et al. 2017; Sikora et al. 2020). Figure 1 presents an illustration of the assumed geometry (see also Figure 3 in Zdziarski et al. 2022, hereafter Z22). The rate of the pairs produced at the base can be compared with the flow rate of nonthermal relativistic electrons emitting synchrotron emission far downstream in the jet. Such a comparison was done for the microquasar MAXI J1820+070, where these two rates were found to be of the same order (Z22).

The ability of loading jets by pairs at their bases was also studied for active galactic nuclei (AGNs) using blazar and/or core-shift models combined with data on their radio lobes (Kang et al. 2014; Sikora 2016; Pjanka et al. 2017). However, this can be tested in some AGNs more directly, in a similar way to that in the case of the microquasar MAXI J1820+070, i.e., by using radio-IR spectra of compact jets and hard X-ray/soft γ-ray spectra of their accretion disk coronae. This is usually not possible in blazars, where the beamed jet emission dominates over the X-rays from accretion. A suitable class of objects is broad-line radio galaxies, where the jet is viewed from a side. We have found the broad-line radio galaxy 3C 120 to be well suited for such calculations.

This is a well-studied, strong, and prominent jet source (Marscher et al. 2002), but at the same time, its X-ray emission is dominated by its accretion flow, as evidenced by the detection of strong reflection features (Zdziarski & Grandi 2001; Lohfink et al. 2013). The model of the broadband jet spectrum from 3C 120 by Janiak et al. (2016) also implies a weak jet contribution to the X-rays. The source was observed about 10 times by the Oriented Scintillation Spectroscopy Experiment (OSSE) detector (Johnson et al. 1993) onboard the Compton Gamma Ray Observatory, whose average spectrum was published by Woźniak et al. (1998), and compared to a number of X-ray observations at lower energies in Zdziarski & Grandi (2001). Apart from a moderate difference in the normalization, the OSSE spectrum (starting at 50 keV) was in

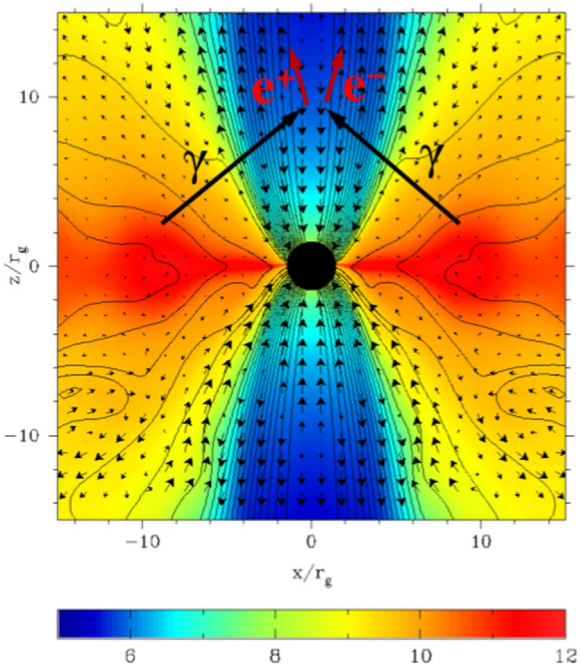

Figure 1. A sketch of the pair-producing geometry based on Figure 2(a) of Barkov & Komissarov (2008), which shows the result of their GRMHD simulation for strongly magnetized accretion on a BH with the mass of $3M_\odot$ and the spin parameter of $a_* = 0.9$. The contours show the magnetic field lines, the arrows show the velocity field, and the color contours show the baryonic rest-mass density, ρ, in a logarithmic scale in $\log_{10}\rho$ in units of g cm^{-3}. The jet base, shown in blue, has a very low matter density. We show $e^\pm$ pair production within the jet base with the arrows representing pair-producing photons and the pairs.

good agreement with that from BeppoSAX (extending up to ≈100 keV) but showed a power-law extension at high energies, with the detection up to ≈400 keV. For the synchrotron spectrum, we use the spectral measurements from radio to IR listed in Giommi et al. (2012).

The redshift to 3C 120 is $z_r = 0.033$, which implies the luminosity distance of $D \approx 141$ Mpc (for $H_0 = 72$ km s^{-1} Mpc^{-1}, $\Omega_\Lambda = 0.7$, and $\Omega_M = 0.3$). The latest determination of its BH mass is $M \approx 6.92^{+2.63}_{-2.45} \times 10^7 M_\odot$ (Grier et al. 2017). It corresponds to the Eddington luminosity of $L_E \approx 1.0 \times 10^{46}$ erg s^{-1} assuming the H mass fraction of $X = 0.7$ and to the gravitational radius of $R_g \equiv GM/c^2 \approx 1.0 \times 10^{13}$ cm. Its accretion luminosity was estimated by Ogle et al. (2005), Kataoka et al. (2011), Zdziarski et al. (2015), and Janiak et al. (2016) as $L_{accr} \approx 1.5$, 0.8, 0.8, and 1.7×10^{45} erg s^{-1}, respectively, which correspond to the Eddington ratio of 0.08–0.17. Given this relatively large ratio, the accretion efficiency, ϵ, is implied to be large, likely in the 0.1–0.3 range. The jet inclination was measured as $i \approx 20.^\circ5 \pm 1.^\circ8$ (Jorstad et al. 2005), $i \approx 16^\circ$ (Agudo et al. 2012), $i \approx 10.^\circ4 \pm 2.^\circ3$ (Jorstad et al. 2017), and $i \approx 18.^\circ7 \pm 0.^\circ5$ (Pushkarev et al. 2017). The average value of the jet Lorentz factor was measured as $\Gamma \approx 5.3 \pm 1.2$ (Jorstad et al. 2005), $\Gamma \approx 10.7 \pm 2.4$ (Jorstad et al. 2017), and $\Gamma \approx 7.9 \pm 0.6$ (Pushkarev et al. 2017). The jet half-opening angle was estimated as $\Theta \approx 3.^\circ8 \pm 1.^\circ3$ (Jorstad et al. 2005), $\Theta \approx 1.^\circ2 \pm 0.^\circ5$ (Jorstad et al. 2017), and $\Theta \approx 3.^\circ1 \pm 0.^\circ1$ (Pushkarev et al. 2017). Based on the above estimates, we will use in this work the following values,

$$i \approx 15^\circ \pm 5^\circ, \quad \Gamma \approx 7.5 \pm 2.5, \quad \Theta \approx 2^\circ \pm 1^\circ, \qquad (1)$$

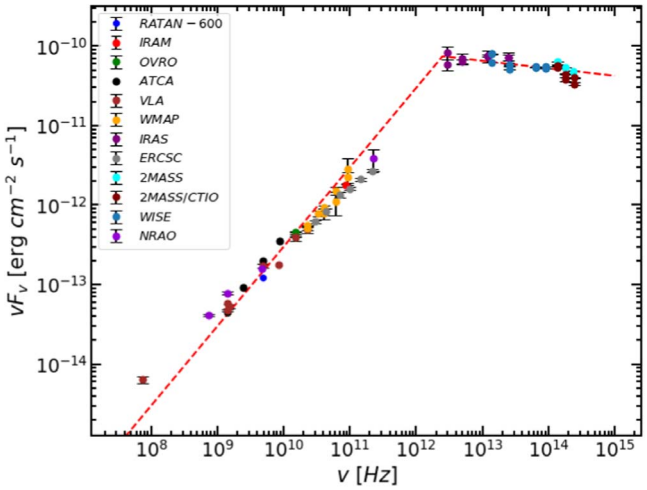

Figure 2. The radio-to-IR spectrum of the core of 3C 120 from various measurements compiled in Giommi et al. (2012). The red dashed line gives a fit of the broken-power-law approximation to the partially synchrotron self-absorbed jet spectrum, Equation (A1).

$$L_{accr} \approx 1.0 \pm 0.2 \times 10^{45}\,\mathrm{erg\ s^{-1}}, \quad \epsilon \approx 0.2 \pm 0.1. \qquad (2)$$

2. The Spectra and Model

Figure 2 shows the radio-to-IR spectrum of the core of 3C 120, representing the inner and steady part of the jet. While the measurements shown were not simultaneous, we see relatively little scatter among them, indicating that the core compact jet is indeed stable. Its radio-to-IR spectrum has a power-law part approximately flat in F_ν (below $\sim 10^{12}$ Hz), followed by a significantly steeper power law at higher frequencies. This implies the presence of a break frequency in between. The low-ν part is usually interpreted as coming from jet synchrotron emission that is partially self-absorbed (Blandford & Königl 1979; Königl 1981), while the part above the break frequency comes from synchrotron emission that is optically thin in the entire emitting part of the jet. There is a possible contribution in the IR from the molecular torus. However, it appears to be negligibly small in 3C 120, which we have inferred based on the quasar template in Richards et al. (2006).

The radio-to-submillimeter part of the spectrum forms a hard power law, which we fitted[4] as $F_\nu \propto \nu^\alpha$ with $\alpha \approx -0.20 \pm 0.04$ (where the uncertainty is 1σ). This fits well its entire range of 74 MHz–226 GHz. However, an extrapolation of this power law to the IR band intersects the softer power law at a frequency a factor of a few above its minimum measured energy. This shows the overall spectrum is more complex than that implied by the model of Blandford & Königl (1979). Namely, the $\alpha \approx -0.20$ radio-to-submillimeter power law has to change to a harder one in order to connect to the lowest IR point. Such changes are related to the rates of change in the density of the relativistic electrons and of the magnetic field strength; see, e.g., Königl (1981) and Zdziarski et al. (2019). However, our goal here is to estimate the rate of the electron flow at the onset of the emitting region (with $z \propto \nu^{-1}$), and we do not need to consider this complexity. Thus, we approximate

[4] Some of the fluxes we compiled from the literature had no measurement errors, and for the χ^2 fit (weighted by inverse squares of the errors) we assumed them to be equal to 5% of the flux.

the overall spectrum as a once-broken power law, with the two parts intersecting around the break frequency. The hard power law has $\alpha_{\rm thick}=0$, and the power law fitted to the IR part of the spectrum has $\alpha_{\rm thin}\approx -1.09\pm 0.02$. This is shown by the dashed line in Figure 2, where we see it still provides a fair approximation to the entire spectrum.

In our modeling, we follow the formulation of the partially synchrotron self-absorbed conical jet model given in Z22, which we summarize in the Appendix below. The break frequency, ν_0, is defined as corresponding to a unit optical depth at the base of the emitting part, z_0. The broken-power-law approximation is given by Equation (A1). For 3C 120, we find ν_0 and F_ν at ν_0, denoted hereafter as F_{ν_0}, as

$$\nu_0\approx 3.15\times 10^3\,{\rm GHz},\quad F_{\nu_0}\approx 3.0\,{\rm Jy}. \tag{3}$$

The hard index of $\alpha_{\rm thick}=0$ corresponds to the canonical (Blandford & Königl 1979) power-law dependencies of the electron number density and the magnetic field strength, $n(z,\,\gamma)=n_0(z/z_0)^{-a}\gamma^{-p}$ (where γ is the electron Lorentz factor), $B(z)=B_0(z/z_0)^{-b}$, respectively, with $b=a/2=1$. The soft index of $\alpha_{\rm thin}=-1.09$ corresponds to the power-law index of the synchrotron-emitting electrons of $p=1-2\alpha_{\rm thin}\approx 3.18$. We also need to set the minimum and maximum values of γ, which we assume to be $\gamma_{\rm min}=2$ (approximately the minimum for which the relativistic formulae are valid) and $\gamma_{\rm max}=10^4$. These values give a low average electron kinetic energy of $\approx 2.7m_{\rm e}c^2$, where $m_{\rm e}$ is the electron mass. Given the relative steepness of the electron distribution, all derived quantities weakly depend on $\gamma_{\rm max}$. Furthermore, we assume the ratio between the energy densities of the matter (kinetic only) and magnetic field of $\beta_{\rm eq}=1$, where we further assume the only contribution to the matter kinetic energy density is from the relativistic electrons; see Equation (A5). We stress, however, that a contribution from ions is possible.

In order to estimate the uncertainty ranges of our derived quantities, we find their extreme values by varying the values of i, Γ, Θ, and $L_{\rm accr}$ in the ranges given in Equations (1)–(2)). Some of those ranges are large, violating the assumptions behind the standard propagation of errors, and thus the above procedure gives more realistic, as well as conservative, error ranges.

Knowing ν_0, F_{ν_0}, p (from the observed spectrum), and D, Γ, i, and Θ (from other observations, Section 1), as well as assuming $\gamma_{\rm min}$, $\gamma_{\rm max}$, and $\beta_{\rm eq}$, we can use standard formulae for the synchrotron emission and absorption and the relativistic transformations and determine the distance of the onset of the emission, z_0, and the magnetic field strength there, B_0; see Equations (A3) and (A4), respectively. For our estimated values, we find

$$z_0\approx 2.0^{+1.3}_{-0.5}\times 10^{16}\,{\rm cm}\approx 1.9^{+1.3}_{-0.4}\times 10^3 R_{\rm g}, \tag{4}$$

$$B_0\approx 47^{+31}_{-17}\,{\rm G}. \tag{5}$$

The dependence of z_0 on $\beta_{\rm eq}$ is very weak, as $\propto\beta_{\rm eq}^{-0.05}$, and also the dependence on $\gamma_{\rm min}$ is weak. Our estimate of z_0 is consistent with the existing estimates of the location of blazar zones (where the bulk of the high-energy emission originates), which are found at distances between those of the broad-line regions and the molecular torii, $\sim 10^3$–$10^5 R_{\rm g}$ (e.g., Madejski & Sikora 2016).

We can compare the above estimate of $B_0(z_0)$ with that using measurements of the core shift, which is an angular displacement of the position of the radio core between two frequencies (Lobanov 1998). It appears that the only such measurements for 3C 120 are those of the angular shift between 2.3 and 8.6 GHz of 1.196 ± 0.018 and 0.956 ± 0.016 mas by Kovalev et al. (2008). To estimate the magnetic field from them, we use Equation (7) of Zdziarski et al. (2015). Using the range of the measured core shift and the assumed Γ, i, and Θ, we find $B_0(z_0)\approx 27$ and 23 G, respectively, with the total uncertainty range of 18–34 G, i.e., about 50% of the values estimated from the break frequency and the flux. Because the two sets of values are estimated based on frequencies separated by a factor of $\sim 10^2$, we consider them to be in relatively good agreement.

Given the values of B_0 and ν_0, we can estimate the electron Lorentz factor corresponding to the bulk of the emission in the partially self-absorbed part—see Equation (16) of Z22—

$$\gamma_{\rm bulk}\approx\left(\frac{B_{\rm cr}}{B_0}\frac{h\nu_0}{\delta m_{\rm e}c^2}\right)^{1/2}\approx 90^{+10}_{-10}, \tag{6}$$

where δ is the Doppler factor, $B_{\rm cr}$ is the critical magnetic field strength, and the numerical value is for our determined parameters. For the validity of the assumed model, $\gamma_{\rm min}$ needs to be a factor of at least a few lower than $\gamma_{\rm bulk}$. This shows $\gamma_{\rm min}$ needs to be relatively low, but it could still be larger than our assumed $\gamma_{\rm min}=2$.

Next, we can calculate the rate of the flow of electrons through the jet, $\dot N_{\rm e}$, which is given by the relativistic number flux; see Equation (A7). Substituting our assumed values and obtained solutions, we find

$$\dot N_{\rm e}\approx 2.7^{+12}_{-2.3}\times 10^{49}\,{\rm s}^{-1}\propto\Theta^{\frac{8+2p}{13+2p}}\gamma_{\rm min}^{\frac{7-12p}{13+2p}}, \tag{7}$$

which is an increasing function of Γ, Θ, and i. The dependence on $\gamma_{\rm min}$ is approximate, valid for $\gamma_{\rm min}\gg 1$.

We then compare the rate of Equation (7) to an estimate of the pair-production rate within the jet base due to collisions of photons from the accretion flow. We use the average OSSE spectrum obtained by Woźniak et al. (1998), shown in Figure 3. For comparison, we also show the average spectrum[5] from Neil Gehrels Swift Burst Alert Telescope (BAT; Oh et al. 2018). Apart from a slightly higher normalization, its part at $\gtrsim$50 keV is compatible with the average from the OSSE. We have fitted the OSSE spectrum by a power law, shown by the red line. We find $\alpha_{\rm X}\approx -1.11^{+0.27}_{-0.26}$ and the normalization of $EF_E(511\,{\rm keV})\approx 0.015^{+0.07}_{-0.05}\,{\rm keV}/({\rm cm}^2\,{\rm s})$, where the uncertainties are 1σ (but $\alpha_{\rm X}$ and EF_E are strongly correlated). This gives us the density of photons within the jet base, Equation (A10). We then calculate the rate of pair production by photons with such a power law, which also depends on the assumed characteristic sizes of the hot plasma, $R_{\rm hot}$, and the jet base, $R_{\rm jet}$; see Equation (A11). From it, we obtain

$$2\dot N_+\approx 3.9^{+6.3}_{-2.8}\times 10^{49}\left(\frac{R_{\rm hot}}{10R_{\rm g}}\right)^{-1}\left(\frac{R_{\rm jet}}{R_{\rm hot}}\right)^2{\rm s}^{-1}. \tag{8}$$

(The given uncertainty is for the 1σ joint $\alpha_{\rm X}$–$EF_E(511\,{\rm keV})$ error contour.) This pair-production rate is then balanced by the sum of the rates of pair annihilation and pair advection. The equilibrium Thomson optical depth of the pairs is of the order of unity. Still, the advection downstream along the jet is likely

[5] https://swift.gsfc.nasa.gov/results/bs105mon/226

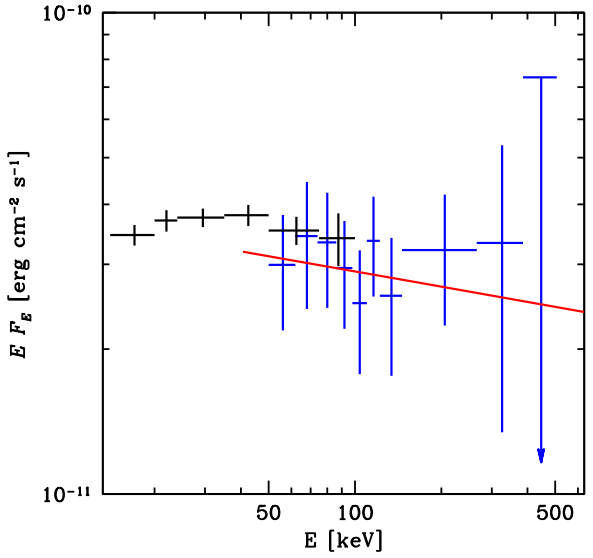

Figure 3. The blue symbols show the average 1992–1997 Compton Gamma Ray Observatory OSSE spectrum of 3C 120 from Woźniak et al. (1998). The red line gives the best power-law fit in the 50–500 keV range. For comparison, we show the 2004–2013 average spectrum (Oh et al. 2018) from the Neil Gehrels Swift BAT (fitted separately by a power law, not shown).

to dominate because the pairs are produced with a substantial net momentum along the jet axis (Beloborodov 1999).

We see that the two rates are similar. This is a remarkable coincidence because the two numbers have been derived with very different physics. This shows that pair production by accretion photons is fully capable of providing most of the leptons responsible for the jet synchrotron emission. The same conclusion was reached for the hard spectral state of the accreting X-ray binary MAXI J1820+070.

Another argument for the presence of $e^{\pm}$ pairs in the source is given by a calculation of the jet power, $P_{\rm j}$. The total jet power in the framework of the theoretically predicted (Bisnovatyi-Kogan & Ruzmaikin 1974, 1976; Narayan et al. 2003) and numerically confirmed (Punsly et al. 2009; Tchekhovskoy et al. 2011; McKinney et al. 2012) magnetically arrested disk (MAD) scenario is

$$P_{\rm j} \approx 1.3(\phi_{\rm BH}/50)^2 a_*^2 \dot{M}c^2, \tag{9}$$

where $\dot{M}$ is the accretion rate, a_* is the BH spin parameter, and $\phi_{\rm BH}$ is a dimensionless magnetic flux threading the BH on one hemisphere related to the dimensional flux by $\Phi_{\rm BH} = \phi_{\rm BH}(\dot{M}c)^{1/2}R_{\rm g}$. GRMHD simulations have shown that $\phi_{\rm BH} \lesssim 50 h_{0.3}^{1/2}$, where $h_{0.3}$ is a dimensionless disk half-thickness defined as $H_{\rm disk} = R_{\rm disk}0.3h_{0.3}$ (Davis & Tchekhovskoy 2020). Noting that $a_* < 1$ and $h_{0.3} \lesssim 1$, $P_{\rm j} \lesssim \dot{M}c^2 \equiv L_{\rm accr}/\epsilon$, which is also a general, model-independent constraint. In 3C 120, we find

$$P_{\rm j} \lesssim 5 \pm 1 \times 10^{45}(\epsilon/0.2)^{-1}{\rm erg\ s^{-1}}. \tag{10}$$

In our model, we can then calculate the jet power in the magnetic field and electrons, P_{Be}, using Equation (A9),

$$P_{Be} \approx 1.5^{+10.2}_{-1.3}(1/2 + \beta_{\rm eq}/3) \times 10^{45}{\rm erg\ s^{-1}}. \tag{11}$$

The power in cold ions associated with electrons not in $e^{\pm}$ pairs is given by Equation (A8). We obtain

$$P_{\rm i} \approx 3.1^{+19.6}_{-2.8} \times 10^{47}(1 - 2n_+/n_{\rm e}){\rm erg\ s^{-1}}, \tag{12}$$

where n_+ and $n_{\rm e}$ are the densities of the positrons and of all leptons, respectively, and in steady state $n_+/n_{\rm e} \approx \dot{N}_+/\dot{N}_{\rm e}$. Both P_{Be} and $P_{\rm i}$ increase with Γ, i, and Θ, while $P_{Be}/P_{\rm i} \approx 0.005/(1 - 2n_+/n_{\rm e})$ (for $\beta_{\rm eq} \approx 1$) remains approximately constant. Thus, the power in the electrons and B is negligible compared to that in the ions unless the jet consists of almost pure pair plasma. Then, $P_{\rm i}/P_{\rm j} \gtrsim 62^{+860}_{-60}(1 - 2n_+/n_{\rm e})$. Thus, the presence of pairs is required by the physical requirement of $P_{\rm i} \leqslant P_{\rm j}$, implying $1 - 2n_+/n_{\rm e} \ll 1$ (i.e., a pair-dominated jet) in most of the parameter space. On the other hand, $P_{\rm i}$ is approximately $\propto \gamma_{\rm min}^{(7-12p)/(13+2p)}$, and thus the pair abundance, $2n_+/n_{\rm e}$, can be close to null if $\gamma_{\rm min} \gg 2$.

The above comparison also implies the jet power of 3C 120 can be near the maximal possible power. In the case of the jet extracting the BH rotational power, we can test this conjecture by comparing the magnetic flux threading the BH with that estimated from the observed synchrotron emission downstream in the jet at $z \geqslant z_0$. The latter was determined for a sample of radio-loud AGNs in Zamaninasab et al. (2014) and Zdziarski et al. (2015). We use Equation (21) in Zdziarski et al. (2015) for the quantities at z_0,

$$\Phi_{\rm j} = 2^{3/2}\pi R_{\rm H} s z_0 B_0 (1 + \sigma_0)^{1/2}/(\ell a_*), \tag{13}$$

where $R_{\rm H} = [1 + (1 - a_*^2)^{1/2}]R_{\rm g}$ is the BH horizon radius, $\ell \lesssim 0.5$ is the ratio of the angular frequencies of the magnetic field lines dragged around the BH and of the BH, $s \lesssim 1$ is defined by

$$\sigma_0 \equiv (\Theta\Gamma/s)^2 \tag{14}$$

(Komissarov et al. 2009; Tchekhovskoy et al. 2009), and σ_0 is the magnetization parameter at z_0. In our estimates below, we adopt $a_* = 1$ and $\ell = 0.5$. We find

$$\Phi_{\rm BH} \approx 2.1 \pm 0.2(\phi_{\rm BH}/50)(\epsilon/0.2)^{-1/2}10^{32}{\rm G\ cm^2}, \tag{15}$$

$$\Phi_{\rm j} \approx 1.7^{+3.0}_{-0.9} s(1 + \sigma_0)^{1/2}10^{32}\ {\rm G\ cm^2}. \tag{16}$$

We thus find here another remarkable coincidence (in agreement with that of Zamaninasab et al. 2014 and Zdziarski et al. 2015) of the two values of the magnetic flux fully compatible with being identical for $\phi_{\rm BH} \sim 50$ and $\sigma_0 \lesssim 1$, expected at $z \gtrsim z_0$. Thus, the jet power can be maximal, corresponding to a jet ejected from a system with an MAD accretion flow and a maximally rotating BH.

Now we consider the value of the magnetization parameter, σ_0. By definition,

$$\sigma_0 \equiv \frac{B_0^2/4\pi}{\eta u_{\rm k,0} + \rho_0 c^2} \approx \frac{B_0^2/4\pi}{n_0 f_N \mu_{\rm e} m_{\rm p} c^2 (1 - 2n_+/n_{\rm e})}, \tag{17}$$

where η is the particle adiabatic index, $u_{\rm k,0}$ is the kinetic energy density of particles at z_0, $\rho_0 c^2$ is the rest-energy density at z_0, f_N is given by Equation (A6), $\mu_{\rm e} = 2/(1 + X)$ is the mean electron molecular weight, and $m_{\rm p}$ is the proton mass. In our case, $u_{\rm k,0} \ll \rho_0 c^2$, e.g., 1/600 of the latter for our default parameters and in the absence of pairs, which in turn leads to the approximate equality on the right-hand side. For our assumed

parameters, we find, using Equations (17) and (14),

$$\sigma_0 \approx \frac{2.5 \times 10^{-3}}{\beta_{\rm eq}(1 - 2n_+/n_{\rm e})}, \tag{18}$$

$$\sigma_0 \approx 6.9^{+20.5}_{-6.1} s^{-2} \times 10^{-2}, \tag{19}$$

respectively, where the former is independent of Γ, i, and Θ. Setting the two values of σ_0 equal implies $(1 - 2n_+/n_{\rm e})\beta_{\rm eq} \ll s^2$, i.e., a pair-dominated plasma for most of the parameter space. For our default values, $2n_+/n_{\rm e} \approx 0.96$, i.e., there are about 25 times more leptons in pairs than in the ionization electrons. We also note that our estimated values of σ_0 are $\ll 1$.

3. Summary and Discussion

We have found that the composition of the jet in 3C 120 is most likely dominated by $e^{\pm}$ pairs. First, a sufficient amount of pairs can be produced by collisions of hard X-rays/soft γ-rays emitted by the accretion flow, as indicated by the estimated rate of pair production being approximately equal to the rate of the flow of synchrotron-emitting electrons downstream in the jet. Second, the high pair content is indicated by the calculation of the jet power, which is dominated by that in the bulk motion of the ions. If the ion density directly corresponds to that of the synchrotron-emitting electrons, the jet power would greatly exceed its maximum possible value, $\dot{M}c^2$, but it can be $\lesssim \dot{M}c^2$ if most of the emitting leptons are those in $e^{\pm}$ pairs. Third, the estimates of the magnetization parameter from the flow parameters and from the product of Θ and Γ agree only at a high pair content. However, apart from the implied result that the pair content, $2n_+/n_{\rm e}$ is ≈ 1, we cannot determine precisely its value because the jet parameters for this source are relatively loosely constrained.

In our calculations, we have assumed the jet is conical in the dissipation zone, at $z \geqslant z_0$, and we have estimated z_0 to equal a few times 10^{16} cm. On the other hand, Kovalev et al. (2020) found that the jet in 3C 120 becomes conical only at distances about 100 times larger. A departure from the conical shape would, however, affect mostly the value of z_0. On the other hand, the parameters of the flow are determined by the jet radius, i.e., Θz_0, which is sensitive mostly to the local synchrotron emission and absorption, and are only weakly affected by the jet shape. Furthermore, we have found the radio-to-submillimeter spectrum forms an almost pure power law at 74 MHz–226 GHz, which indicates that the shape of the jet in the emitting range, which starts relatively close to z_0 (because $z \propto \nu^{-1}$ and 226 GHz is $\sim 0.1\nu_0$), is most likely conical and cannot have a substantial curvature.

Another uncertainty in the assumptions is regarding the low-energy end of the electron distribution. On one hand, the value of $\gamma_{\rm min}$ is uncertain and can be higher than our assumed $\gamma_{\rm min} = 2$. In this case, it will be even easier for the pair production at the jet base to produce enough leptons for the synchrotron emission, while it would reduce the jet power. On the other hand, we expect the presence of a quasi-thermal electron distribution below $\gamma_{\rm min}$ (regardless of its value), which would increase the rate of the electron flow, $\dot{N}_{\rm e}$. Depending on the relative fraction of the electrons in the quasi-thermal part, the value of $\gamma_{\rm min}$, and other jet parameters, this may result in the pair-production rate not being sufficient to account for the full flow. Such a quasi-thermal distribution is expected in the presence of shock acceleration (e.g., Sironi & Spitkovsky 2009; Sironi et al. 2015; Crumley et al. 2019). For acceleration via magnetic field reconnection, simulations performed for $\sigma \geqslant 1$ show the quasi-thermal part to be modest, with the lepton number still dominated by the power-law part (e.g., Comisso & Sironi 2018, 2019; Petropoulou et al. 2019). Furthermore, the presence of substantial excesses of cold electrons in jets of radio-loud AGNs (hence also in 3C 120) is ruled out by the observed absence of soft X-ray excesses in the spectra of blazars. Such an excess would result from the Comptonization of external UV radiation by the cold electrons in a relativistic jet (Sikora et al. 1997).

We thank G. Henri, A. Levinson, P.-O. Petrucci, and T. Savolainen for valuable discussions; the referee for a valuable suggestion; M. Barkov for the permission to use his figure in our illustration of the effect of pair production; and P. Lubiński and N. Żywucka for help with software. We acknowledge support from the Polish National Science Center under the grants 2015/18/A/ST9/00746 and 2019/35/B/ST9/03944. The work of M.B. was supported in part by the National Research Foundation[6] of South Africa (DSI/NRF SARChI Programme, Grant No. 64789).

Appendix
Formulae

In order to make this work self-contained, we present the formulae from Z22 and Zdziarski et al. (2021) that are used here. In Z22, they were given for arbitrary power-law dependencies of $n(z)$ and $B(z)$, while here we give them for the canonical case of $b = a/2 = 1$.

We rewrite Equations (12)–(13) of Z22 as

$$F_\nu \simeq F_{\nu_0} \min\left[1, \frac{5(\nu/\nu_0)^{\frac{1-p}{2}}}{(p-1)\Gamma\left(\frac{p-1}{p+4}\right)}\right], \tag{A1}$$

$$\tau(\nu, z) = [(\nu/\nu_0)(z/z_0)]^{-(p+4)/2}, \tag{A2}$$

which give a broken-power-law approximation to the synchrotron spectrum and the self-absorption optical depth, respectively. Here ν_0 is defined by $\tau(\nu_0, z_0) = 1$, i.e., the jet has $\tau < 1$ at $\nu > \nu_0$ in the entire synchrotron-emitting part, $z \geqslant z_0$, and the two power laws intersect at a $\nu < \nu_0$. Note that $F_{\nu_0} \equiv (2/5)\Gamma[(p-1)/(p+4)]F_0$, where F_0 is defined by Equation (7) of Z22. We then use Equations (A2) and (A4) of Z22, which give the solutions for z_0 and B_0, respectively,

$$z_0 = \frac{1}{\delta^{\frac{4+p}{13+2p}}\nu_0}\left[\frac{c(1+k_{\rm i})(f_E - f_N)}{2\pi\beta_{\rm eq}}\right]^{\frac{1}{13+2p}} \times \left[\frac{C_2(p)}{\sin i}\right]^{\frac{5+p}{13+2p}}\left[\frac{5F_{\nu_0}D^2}{m_{\rm e}C_1(p)\Gamma\left(\frac{p-1}{p+4}\right)}\right]^{\frac{6+p}{13+2p}} \times \left(\frac{3}{\pi\tan\Theta}\right)^{\frac{7+p}{13+2p}}(1+z_{\rm r})^{-\frac{19+3p}{13+2p}}, \tag{A3}$$

[6] Any opinion, finding and conclusion or recommendation expressed in this material is that of the authors, and the NRF does not accept any liability in this regard.

$$B_0 = \left[\frac{3C_1(p)\Gamma\left(\frac{p-1}{p+4}\right)(1+k_{\rm i})^2(f_E-f_N)^2\sin^3 i}{5C_2(p)^3\beta_{\rm eq}^2 D^2 F_{\nu_0}\tan\Theta}\right]^{\frac{2}{13+2p}} \times \frac{\nu_0\pi^{\frac{7+2p}{13+2p}}2^{\frac{9+2p}{13+2p}}c^{\frac{17+2p}{13+2p}}m_{\rm e}^{\frac{15+2p}{13+2p}}(1+z_{\rm r})^{\frac{15+2p}{13+2p}}}{e\delta^{\frac{3+2p}{13+2p}}}, \quad \text{(A4)}$$

where e is the electron charge, and $C_{1,2}$ are constants defined in Equations (8) and (9) of Z22, respectively,

$$\beta_{\rm eq} = \frac{n_0 m_{\rm e} c^2(1+k_{\rm i})(f_E-f_N)}{B_0^2/8\pi}, \quad \text{(A5)}$$

$$f_E \equiv \begin{cases}\dfrac{\gamma_{\rm max}^{2-p}-\gamma_{\rm min}^{2-p}}{2-p}, & p\neq 2;\\ \ln\dfrac{\gamma_{\rm max}}{\gamma_{\rm min}}, & p=2,\end{cases} \qquad f_N \equiv \frac{\gamma_{\rm min}^{1-p}-\gamma_{\rm max}^{1-p}}{p-1}, \quad \text{(A6)}$$

and $k_{\rm i}$ accounts for the kinetic energy density in particles other than the power-law electrons.

The total lepton flow rate and the usable power in ions are

$$\dot{N}_{\rm e} \approx 2\pi n_0 f_N c\beta\Gamma(z0\tan\Theta)^2\,, \quad \text{(A7)}$$

$$P_{\rm i} = \mu_{\rm e} m_{\rm p} c^2(\Gamma-1)(\dot{N}_{\rm e}-2\dot{N}_+), \quad \text{(A8)}$$

respectively, where β is the dimensionless bulk velocity, and both the jet and counterjet are taken into account; see Equations (25)–(26) of Z22. The power in the relativistic electrons and magnetic fields is—see Equation (23) of Z22—

$$P_{Be} = \left(\frac{1}{2}+\frac{\beta_{\rm eq}}{3}\right)c\beta(B_0 z_0\Gamma\tan\Theta)^2\,. \quad \text{(A9)}$$

We then provide the formalism for calculating the pair-production rate, based on Zdziarski et al. (2021). We modify their Equation (1) to calculate the differential photon density at 511 keV, n_1, above the hot disk,

$$n_1 \approx F_E(511\ {\rm keV})\frac{4\pi D^2}{2\pi R_{\rm hot}^2 c}, \quad \text{(A10)}$$

where we divided the total rate of the photon emission by the source area (including both sides), and both F_E and E have the same energy unit (e.g., keV). We then use Equation (3) of Zdziarski et al. (2021), which uses the rate derived by Svensson (1987), and approximate the pair-producing volume as two cylinders with the height $R_{\rm hot}$ and the characteristic radius of the jet, $R_{\rm jet}$ ($\leqslant R_{\rm hot}$), i.e., $V = 2\pi R_{\rm jet}^2 R_{\rm hot}$. We then get the total pair-production rate as

$$\dot{N}_+ \approx 2\pi R_{\rm jet}^2 R_{\rm hot} n_1^2 \sigma_{\rm T} c\frac{\ln(E_{\rm c}/511\ {\rm keV})}{(1-\alpha_{\rm X})^{5/3}(2-\alpha_{\rm X})}, \quad \text{(A11)}$$

where $\sigma_{\rm T}$ is the Thomson cross section, and $E_{\rm c}$ is the upper cutoff of the photon power law, which we assume to be ≈2 MeV.

ORCID iDs

Andrzej A. Zdziarski https://orcid.org/0000-0002-0333-2452
Dakalo G. Phuravhathu https://orcid.org/0000-0002-0870-4569
Marek Sikora https://orcid.org/0000-0003-1667-7334
Markus Böttcher https://orcid.org/0000-0002-8434-5692
James O. Chibueze https://orcid.org/0000-0002-9875-7436

References

Agudo, I., Gómez, J. L., Casadio, C., Cawthorne, T. V., & Roca-Sogorb, M. 2012, ApJ, 752, 92
Aharonian, F. A., Barkov, M. V., & Khangulyan, D. 2017, ApJ, 841, 61
Barkov, M. V., & Komissarov, S. S. 2008, MNRAS, 385, L28
Beloborodov, A. M. 1999, MNRAS, 305, 181
Bisnovatyi-Kogan, G. S., & Ruzmaikin, A. A. 1974, Ap&SS, 28, 45
Bisnovatyi-Kogan, G. S., & Ruzmaikin, A. A. 1976, Ap&SS, 42, 401
Blandford, R. D., & Königl, A. 1979, ApJ, 232, 34
Blandford, R. D., & Znajek, R. L. 1977, MNRAS, 179, 433
Comisso, L., & Sironi, L. 2018, PhRvL, 121, 255101
Comisso, L., & Sironi, L. 2019, ApJ, 886, 122
Crumley, P., Caprioli, D., Markoff, S., & Spitkovsky, A. 2019, MNRAS, 485, 5105
Davis, S. W., & Tchekhovskoy, A. 2020, ARA&A, 58, 407
Ghisellini, G. 2012, MNRAS, 424, L26
Giommi, P., Polenta, G., Lähteenmäki, A., et al. 2012, A&A, 541, A160
Goldreich, P., & Julian, W. H. 1969, ApJ, 157, 869
Grier, C. J., Pancoast, A., Barth, A. J., et al. 2017, ApJ, 849, 146
Henri, G., & Pelletier, G. 1991, ApJL, 383, L7
Janiak, M., Sikora, M., & Moderski, R. 2016, MNRAS, 458, 2360
Johnson, W. N., Kinzer, R. L., Kurfess, J. D., et al. 1993, ApJS, 86, 693
Jorstad, S. G., Marscher, A. P., Lister, M. L., et al. 2005, AJ, 130, 1418
Jorstad, S. G., Marscher, A. P., Morozova, D. A., et al. 2017, ApJ, 846, 98
Kang, S.-J., Chen, L., & Wu, Q. 2014, ApJS, 215, 5
Kataoka, J., Stawarz, Ł., Takahashi, Y., et al. 2011, ApJ, 740, 29
Komissarov, S. S., Vlahakis, N., Königl, A., & Barkov, M. V. 2009, MNRAS, 394, 1182
Königl, A. 1981, ApJ, 243, 700
Kovalev, Y. Y., Lobanov, A. P., Pushkarev, A. B., & Zensus, J. A. 2008, A&A, 483, 759
Kovalev, Y. Y., Pushkarev, A. B., Nokhrina, E. E., et al. 2020, MNRAS, 495, 3576
Levinson, A., & Rieger, F. 2011, ApJ, 730, 123
Liodakis, I., Blinov, D., Potter, S. B., & Rieger, F. M. 2022, MNRAS, 509, L21
Lobanov, A. P. 1998, A&A, 330, 79
Lohfink, A. M., Reynolds, C. S., Jorstad, S. G., et al. 2013, ApJ, 772, 83
Madejski, G. G., & Sikora, M. 2016, ARA&A, 54, 725
Marscher, A. P., Jorstad, S. G., Gómez, J.-L., et al. 2002, Natur, 417, 625
McKinney, J. C., Tchekhovskoy, A., & Blandford, R. D. 2012, MNRAS, 423, 3083
Mościbrodzka, M., Gammie, C. F., Dolence, J. C., & Shiokawa, H. 2011, ApJ, 735, 9
Narayan, R., Igumenshchev, I. V., & Abramowicz, M. A. 2003, PASJ, 55, L69
Nokhrina, E. E., Beskin, V. S., Kovalev, Y. Y., & Zheltoukhov, A. A. 2015, MNRAS, 447, 2726
Ogle, P. M., Davis, S. W., Antonucci, R. R. J., et al. 2005, ApJ, 618, 139
Oh, K., Koss, M., Markwardt, C. B., et al. 2018, ApJS, 235, 4
Petropoulou, M., Sironi, L., Spitkovsky, A., & Giannios, D. 2019, ApJ, 880, 37
Pjanka, P., Zdziarski, A. A., & Sikora, M. 2017, MNRAS, 465, 3506
Punsly, B., Igumenshchev, I. V., & Hirose, S. 2009, ApJ, 704, 1065
Pushkarev, A. B., Kovalev, Y. Y., Lister, M. L., & Savolainen, T. 2017, MNRAS, 468, 4992
Richards, G. T., Lacy, M., Storrie-Lombardi, L. J., et al. 2006, ApJS, 166, 470
Sikora, M. 2016, Galax, 4, 12
Sikora, M., Madejski, G., Moderski, R., & Poutanen, J. 1997, ApJ, 484, 108
Sikora, M., Nalewajko, K., & Madejski, G. M. 2020, MNRAS, 499, 3749
Sironi, L., Petropoulou, M., & Giannios, D. 2015, MNRAS, 450, 183
Sironi, L., & Spitkovsky, A. 2009, ApJ, 698, 1523
Snios, B., Nulsen, P. E. J., Wise, M. W., et al. 2018, ApJ, 855, 71
Svensson, R. 1987, MNRAS, 227, 403
Tchekhovskoy, A., McKinney, J. C., & Narayan, R. 2009, ApJ, 699, 1789
Tchekhovskoy, A., Narayan, R., & McKinney, J. C. 2011, MNRAS, 418, L79
Woźniak, P. R., Zdziarski, A. A., Smith, D., Madejski, G. M., & Johnson, W. N. 1998, MNRAS, 299, 449
Zamaninasab, M., Clausen-Brown, E., Savolainen, T., & Tchekhovskoy, A. 2014, Natur, 510, 126
Zdziarski, A. A., & Grandi, P. 2001, ApJ, 551, 186
Zdziarski, A. A., Jourdain, E., Lubiński, P., et al. 2021, ApJL, 914, L5
Zdziarski, A. A., Sikora, M., Pjanka, P., & Tchekhovskoy, A. 2015, MNRAS, 451, 927
Zdziarski, A. A., Stawarz, Ł., Sikora, M., et al. 2019, MNRAS, 485, 1210
Zdziarski, A. A., Tetarenko, A. J., & Sikora, M. 2022, ApJ, 925, 189